# Ionized gas discs in elliptical and S0 galaxies at $z < 1$

Yara L. Jaffé,[1]★ Alfonso Aragón-Salamanca,[2] Bodo Ziegler,[3] Harald Kuntschner,[4] Dennis Zaritsky,[5] Gregory Rudnick,[6] Bianca M. Poggianti,[7] Carlos Hoyos,[8] Claire Halliday[9] and Ricardo Demarco[1]

[1]*Department of Astronomy, Universidad de Concepción, Casilla 160-C, Concepción, Chile*
[2]*School of Physics and Astronomy, The University of Nottingham, University Park, Nottingham NG7 2RD, UK*
[3]*Department of Astrophysics, University of Vienna, Türkenschanzstr. 17, 1180 Wien, Austria*
[4]*European Southern Observatory, Karl-Schwarzschild Strasse 2, D-85748 Garching, Germany*
[5]*University of Arizona, 933 N. Cherry Ave, Tucson, AZ 85721, USA*
[6]*Department of Physics and Astronomy, The University of Kansas, Malott room 1082, 1251 Wescoe Hall Drive, Lawrence, KS 66045, USA*
[7]*INAF-Osservatorio Astronomico di Padova, vicolo dell Osservatorio 5, I-35122 Padova, Italy*
[8]*Departamento de Astronomia, Instituto de Astronomia, Geofísica e Ciências Atmosféricas da Universidade de São Paulo, Rua do Matão 1226, Cidade Universitária, 05508-090, São Paulo, Brazil*
[9]*23, rue d'Yerres, F-91230 Montgeron, France*

## ABSTRACT

We analyse the extended, ionized-gas emission of 24 early-type galaxies (ETGs) at $0 < z < 1$ from the ESO Distant Cluster Survey (EDisCS). We discuss different possible sources of ionization and favour star formation as the main cause of the observed emission. 10 galaxies have disturbed gas kinematics, while 14 have rotating gas discs. In addition, 15 galaxies are in the field, while 9 are in the infall regions of clusters. This implies that, if the gas has an internal origin, this is likely stripped as the galaxies get closer to the cluster centre. If the gas instead comes from an external source, then our results suggest that this is more likely acquired outside the cluster environment, where galaxy–galaxy interactions more commonly take place. We analyse the Tully–Fisher relation of the ETGs with gas discs, and compare them to EDisCS spirals. Taking a matched range of redshifts, $M_B < -20$, and excluding galaxies with large velocity uncertainties, we find that, at fixed rotational velocity, ETGs are 1.7 mag fainter in $M_B$ than spirals. At fixed stellar mass, we also find that ETGs have systematically lower specific star formation rates than spirals. This study constitutes an important step forward towards the understanding of the evolution of the complex ISM in ETGs by significantly extending the look-back-time baseline explored so far.

**Key words:** galaxies: elliptical and lenticular, cD – galaxies: evolution – galaxies: formation – galaxies: ISM – galaxies: kinematics and dynamics.

## 1 INTRODUCTION

On the basis of their observed properties, early-type galaxies (ETGs) have long been regarded as a homogeneous population of passively evolving galaxies. For example, ETGs follow a tight correlation between colour and magnitude (Baum 1959; Visvanathan & Sandage 1977) that distinguishes them from the (blue) population of spiral and irregular galaxies. The small scatter about this relation suggests a predominantly old stellar population (Bower, Lucey & Ellis 1992; Aragón-Salamanca et al. 1993; Jaffé et al. 2011a). Furthermore, ETGs present a striking correlation between their effective radius, mean surface brightness, and velocity central dispersion (the Fundamental Plane; e.g. Djorgovski & Davis 1987; Dressler et al. 1987; Faber et al. 1987). Combined evidence from studies of the Faber–Jackson, Mgb-$\sigma$, Fundamental Plane, and line strengths provide support for the passive evolution of cluster ETGs (see e.g. Ziegler et al. 2001; Fritz, Böhm & Ziegler 2009, and references therein). Finally, studies of the chemical composition and alpha enhancement in galaxies have shown that more massive galaxies tend to be more metal rich and have a shorter star formation time-scale (Thomas et al. 2005).

However, the idea that ETGs are red and dead systems, essentially devoid of gas and dust, has been questioned in the last decades. Owing to an increase in instrumental sensitivity, a number of observations have gradually revealed the presence of a complex

★ E-mail: yara.jaffe@astro-udec.cl

interstellar medium (ISM) in ETGs. Some examples include the detection of hot gas through X-rays (Forman et al. 1979; O'Sullivan, Forbes & Ponman 2001; Macchetto et al. 1996), H I gas (e.g. Verdes-Montenegro et al. 2001; Gopal-Krishna et al. 2012), warm ionized gas (Demoulin-Ulrich, Butcher & Boksenberg 1984; Kim 1989; Trinchieri & di Serego Alighieri 1991; Kehrig et al. 2012), and dust (Rowlands et al. 2012; di Serego Alighieri et al. 2013). In this context, Trager et al. (2000) proposed a 'frosting' model in which the apparently young ages inferred for some ellipticals by single stellar population models, is due to a 'frosting' of younger stars in a primarily old stellar population (but see Maraston & Thomas 2000). More recently, significant advances have been made in the study of ETGs by the SAURON and ATLAS$^{3D}$ Collaboration using integral-field spectroscopy (see Cappellari et al. 2011, for a recent overview). Their studies of local E/S0s confirmed that emission is commonly found in the central regions of elliptical galaxies and even more so in S0s (e.g. Phillips et al. 1986; Macchetto et al. 1996; Sarzi et al. 2006; Yan et al. 2006), and also revealed a great level of complexity in the internal kinematics of these galaxies. Their most robust explanation for the gas found in some of these galaxies is that it has been accreted from an external source, owing to the co-existence of co- and counter-rotating components of both the gas and the stars in many cases (Shapiro et al. 2010).

In spite of all these efforts, the origin and state of the gas in ETGs remains a puzzle. Many studies have been devoted to understanding the source of the gas ionization in ETGs (Binette et al. 1994; Stasińska et al. 2008; Sarzi et al. 2010; Annibali et al. 2010; Finkelman et al. 2010; Kehrig et al. 2012). Different excitation mechanisms have been proposed, including photoionization of ISM by either post asymptotic giant branch (AGB) stars, shocks, active galactic nuclei (AGN), or OB stars. It remains unclear, however, the degree to which these processes contribute to the ISM ionization of ETGs

One way to understand the formation and evolution of ETGs is by studying their scaling relations (e.g. the Fundamental Plane, Faber–Jackson relation, or colour–magnitude relation, see Renzini 2006, for a review) as a function of redshift, environment, and intrinsic galaxy properties (e.g. van der Wel et al. 2004; Jørgensen et al. 2006; Saglia et al. 2010; Jaffé et al. 2011a). To further understand the evolutionary link between the different galaxy types, it is also useful to investigate the location of ETGs in the late-type galaxy scaling relations. For disc galaxies, an especially useful relation is the Tully–Fisher relation (TFR; Tully & Fisher 1977), which relates the disc luminosity to the maximum rotational velocity of disc galaxies. Studies of the TFR as a function of morphology have shown significant differences between E/S0 and spiral galaxies. Gerhard et al. (2001) studied the TFR of nearly round elliptical galaxies and found that they follow a TFR with marginally shallower slope than spiral galaxies and ∼1 mag fainter zero-point in the *B* band. Bedregal, Aragón-Salamanca & Merrifield (2006) also found an offset in the TFR of S0s and spirals. Naively, this offset can be interpreted as the result of the fading of spiral galaxies since they ceased forming stars. The large intrinsic scatter however suggests that the S0s cannot have simply faded after having (all) transformed at a single epoch. They conclude that the scatter in the S0 TFR arises from the different times at which galaxies began their transformation. More recently, Williams, Bureau & Cappellari (2010) performed a careful study of the S0 TFR also finding an offset between the spiral and the S0 TFR. They extensively analyse biases and obtain a smaller (but still significant) TFR offset than in Bedregal et al. (2006). They conclude from their study that this offset can be explained if S0s are systematically smaller or more concentrated than spirals. However,

the recent study of Rawle et al. (2013) of Coma spirals and S0s essentially confirms the conclusions and interpretation of Bedregal et al. (2006). Moreover, they find that the amount of fading experienced by the S0s is correlated not only with the time since the cessation of star formation, but also with the time of accretion into the cluster, clearly indicating that the transformation of spirals to S0s is accelerated by cluster environment.

All of the above-mentioned studies however have been done at low redshift. In this paper, we present, for the first time, observational evidence for extended emission discs in ETGs at intermediate redshift ($0 < z < 1$) and perform a comparison with similarly selected emission-line spirals.

In Jaffé et al. (2011b), we studied the gas kinematics (from emission lines), morphological disturbances, and the TFR of distant galaxies as a function of environment using the ESO Distant Cluster Survey (EDisCS). In our analysis, the vast majority of the emission-line galaxies were spirals and irregulars. However, we found that a significant number of ETGs at $0 < z < 1$ have extended emission in their spectra. Such high-redshift objects, which have not yet been studied, are the primary focus of this paper. In Section 2, we summarize the EDisCS data and the parent sample of Jaffé et al. (2011b). We present the emission-line ETG sample in Section 3, along with their gas dynamics and stellar morphologies. In Section 4, we explore the possible mechanisms responsible for ionizing the gas in the emission-line ETGs, and then study their environments, TFR, and specific star formation rates (SFRs). We then discuss our results in Section 5 and summarize our main findings and conclusions in Section 6.

## 2 THE PARENT SAMPLE

The galaxies used in the analysis of this paper are drawn from the sample used in Jaffé et al. (2011b), which consists of emission-line galaxies from the EDisCS. We summarize the EDisCS dataset briefly in Section 2.1 and the sub-sample of Jaffé et al. (2011b) in Section 2.2, but refer to the original papers for a full description.

### 2.1 EDisCS

EDisCS is a multiwavelength survey of 20 fields containing galaxy clusters at redshifts between 0.4 and 1. The cluster sample was selected from 30 of the highest surface-brightness candidates in the Las Campanas Distant Cluster Survey (Gonzalez et al. 2001).

The dataset includes optical photometry (see White et al. 2005) from FORS2 on the Very Large Telescope (VLT) in *B*, *V*, and *I* band for the 10 intermediate-redshift cluster candidates and *V*, *R*, and *I* bands for the 10 high-redshift cluster candidates. In addition, near-IR *J* and *K* photometry was obtained for most clusters using SOFI at the New Technology Telescope (Aragón-Salamanca et al., in preparation). We also compiled deep multislit spectroscopy with FORS2/VLT (Halliday et al. 2004; Milvang-Jensen et al. 2008), which consists of high signal-to-noise data for ∼30–50 members per cluster and a comparable number of field galaxies in each field down to $I = 22$ and 23 for the mid- and high-redshift clusters, respectively. The wavelength range was typically ∼5300–8000 Å for two of the runs and 5120–8450 Å for the other two. Cluster and field galaxies were separated using spectroscopic redshifts (see Milvang-Jensen et al. 2008 for details).

In addition to this, for 10 of the higher redshift clusters from the data base we acquired *Hubble Space Telescope* (*HST*) mosaic images in the *F814W* filter with the Advanced Camera for Surveys Wide Field Camera (see Desai et al. 2007 for details).

## 2.2 The emission-line galaxy sample of Jaffé et al. (2011b)

To construct a TFR, in Jaffé et al. (2011b), we used a sub-sample of the EDisCS dataset consisting of galaxies with measurable emission in their spectra (typically the [O II]3727 Å doublet, Hβ, the [O III]4959 and 5007 Å lines, Hγ, and/or Hδ). Given the two-dimensional (2D) nature of the spectra, this selection was carried out by the careful visual inspection of each emission line. Subsequent quantitative analysis of the S/N of these lines revealed that in the majority of cases the fraction of pixels whose signal was larger than $2\sigma$ above the noise was over 95 per cent of all the detected pixels (i.e. those pixels accepted by the fitting procedure). To ensure that rotation could be measured, we rejected galaxies with inclinations of less than $30°$ (inclination = 0 corresponding to face-on). We also rejected observations affected by slit misalignment (misalignment with respect to the major axis of the galaxy $>30°$). After applying these selection criteria, we built a sample of 422 galaxies with 1024 emission lines in total.

The 'true' parent emission-line galaxy distribution is well represented by this sample. The fraction of EDisCS galaxies with emission-line spectra for which we were able to model emission lines and measure a rotation curve is fairly constant ($\simeq 35$ per cent) across the magnitude range of our galaxies.

In Desai et al. (2007), galaxy morphologies were assigned by the visual inspection of *HST* images by a team of expert classifiers. The *HST* data however only cover about half of the full spectroscopic sample. For the *HST* sub-sample, we found that the morphology distribution of the emission-line galaxies was dominated by spirals and irregulars (see fig. 8 in Jaffé et al. 2011b), although we identified 44 galaxies with E/S0 morphology.

# 3 THE EMISSION-LINE ETG SAMPLE OF THIS PAPER

In Jaffé et al. (2011b), we focused mainly on the visually classified spiral galaxies within the emission-line galaxy sample of Section 2.2. This paper focuses now on the ETGs. We apply the selection used in Jaffé et al. (2011b, see also Section 2.2) to create the emission-line sample, and using the visual morphologies of Desai et al. (2007), we identify 44 ETG candidates with emission lines (27 E and 17 S0). To ensure that the morphologies were reliable, three co-authors (YJ, AAS, and CHo) carefully re-examined the *HST* images and found that three galaxies were incorrectly classified as E/S0. Taking these misclassifications out of the sample, we were left with 41 ETGs, which is the sample considered in this paper. Table A1 shows the main properties of these galaxies, including the three misclassified ones.

## 3.1 Emission-line kinematics

To make sure that the emission in the ETG sample is real, and to study the gas kinematics, we carefully inspected the 2D emission-lines of each galaxy spectra, as well as the residuals resulting from subtracting 2D fits to each line, in the same manner as in Jaffé et al. (2011b). When checking the spectra, we found that only 24 of the 41 ETGs have real emission. The remaining 17 galaxies present 'artificial emission' that is likely the result of artefacts in the 2D spectra and were thus discarded (e.g. a poorly subtracted overlapping sky line or cosmic rays; see discussion in Jaffé et al. 2011b). We further inspected the kinematics of the galaxies with real emission and found that 14 have undisturbed (rotating) disc kinematics, and 10 have clear asymmetries in their emission-line

profiles (i.e. disturbed kinematics), as shown in Figs B1 and B2, respectively. As explained in Jaffé et al. (2011b), rotation velocities could only be safely computed for those galaxies with undisturbed disc kinematics. For those galaxies, however, the emission was typically quite extended (~2–5 times the photometric scalelength for S0s and ellipticals, respectively, see fig. 21 in Jaffé et al. 2011b), so a reliable rotation velocity could be measured. In terms of the effective radius ($r_{\rm eff}$), the emission in these ETGs typically extends up to $1$–$5 \times r_{\rm eff}$ (see columns 9 and 10 of Table A1).

Unfortunately, with the available data, we cannot measure the velocity dispersion (of either the gas or the stars) for our sample.

## 3.2 The final emission-line ETG sample

After the morphological and dynamical inspections, the final true emission-line ETG sample consists of 24 galaxies, that is, 14 ellipticals and 10 S0s, among which 14 have undisturbed and 10 disturbed kinematics. Their main properties are listed in the top part of Table A1. Note that two of the galaxies in the final sample are a close pair (EDISCS ID's have an appended '_A' and '_B') and hence, suffer from mutual light contamination. For this reason, although we include these galaxies in our sample, we do not analyse their individual kinematics.

Figs B1 and B2 show the *HST* postage-stamp images of all the emission-line ETGs in our sample, as well as their single-Sérsic model and residuals (cf. Section 4.3), 2D spectra and emission-line model.

As Fig. 1 shows, our sample spans a broad range of redshifts and absolute rest-frame $B$-band magnitudes ($M_B$, corrected for Galactic extinction). Values of $M_B$ were calculated from the observed spectral energy distribution of each galaxy, normalized to its total $I$-band flux, and the spectroscopic redshift (see Rudnick et al. 2009 for details). The distribution of ETGs in this plot is very similar to that of the spirals. In Jaffé et al. (2011b), we defined a 'matched sample' of cluster and field galaxies by imposing the following magnitude
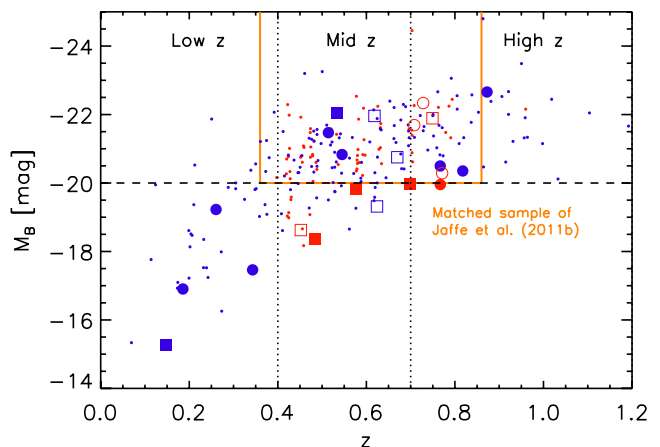


**Figure 1.** Redshift versus $M_B$ for the parent emission-line sample with spiral morphology (small dots), and the ETG sample (larger symbols). In both cases, blue symbols correspond to field galaxies and red ones to galaxies in clusters or groups. For the ETG sample, we have distinguished elliupticals (circles) from S0s, as well as galaxies with disturbed (open symbols) and undisturbed kinematics (filled symbols). The solid orange box corresponds to the matched sample used in Jaffé et al. (2011b, sample 'C'). The vertical dashed lines indicate the different redshift ranges used in the analysis of this paper (e.g. Figs 4 and 5), whilst the horizontal dashed line places a reasonable $M_B$ limit to compare the galaxies across all redshifts.

and redshift cuts: $M_B < -20$ and $0.35 < z < 0.86$ (orange square in the figure). Owing to the broader redshift range of the ETGs considered in this paper and the small number of galaxies, we define three redshift bins (low, intermediate, and high) to pursue our comparative analysis (cf. Section 4). These are separated by vertical dotted lines in Fig. 1. We indicate with a horizontal dashed line the magnitude limit up to which we can reliably compare galaxies at all redshifts ($M_B = -20$). This line was chosen to roughly match the completeness of the sample across all the redshifts considered.

We emphasize that, within the matched sample of Jaffé et al. (2011b, yellow box in Fig. 1), ETGs with emission lines are quite rare: only ~12 per cent of the emission-line galaxies have early-type morphology. Conversely, about 18 per cent of E/S0s in the matched sample have detected emission lines. It is likely, however, that ETGs with either weak emission lines or slit misalignments were rejected from our selection (more so than spirals). Hence, the true fraction of ETGs with gas discs is likely larger than our estimate.

## 4 RESULTS

We first explore the possible sources of ionization of the ETGs presented in Section 3.2, and then study their environments, morphological disturbances, TFR, and specific SFRs (sSFRs).

### 4.1 Source of ionization

We have considered three different possible causes for the ionization of the gas in ETGs, namely (i) AGN activity, (ii) star formation, or (iii) post-AGB stars. Although the available FORS2 spectra are not ideal to unambiguously test the possible scenarios, we discuss each case below and place some constraints.

In Poggianti et al. (2006), it was estimated that the contamination from pure AGN in the EDisCS spectroscopic sample is at most 7 per cent. Although this is a statistical result, it is unlikely that all of our ETGs belong to this 7 per cent minority. Owing to the limited spectral coverage of most of our spectra, we are unable to identify AGN using a BPT diagram (Baldwin, Phillips & Terlevich 1981). However, following Sánchez-Blázquez et al. (2009), we investigated, when possible, the ratio of [O II] to H$\beta$. For the two ETGs with detected [O II] and H$\beta$, we find that [O II]/H$\beta$ is much lower than 6.7, the limit below which the emission is considered to be powered by star formation (based on the condition [O II]/H$\alpha$ < 1.5, from Kewley, Geller & Jansen 2004). Moreover, AGN are expected to exhibit centrally concentrated nuclear emission, contrary to what we observe in our ETG sample (see Figs B1 and B2, and Table A1). Notwithstanding the limited available evidence, we are inclined to favour star formation over AGN activity.

The other possibility is that the ionization of the gas in ETGs is mainly caused by hot evolved stars rather than young ones (Trinchieri & di Serego Alighieri 1991). This scenario has been largely debated in recent years (see e.g. Boselli et al. 2005; Yi et al. 2011; Zaritsky, Gil de Paz & Bouquin 2014, and references therein) and has received strong observational support from various studies (Yan & Blanton 2012, and references therein). In particular, Binette et al. (1994) showed that, over a wide range of ionization parameteres, photoionization by post-AGB stars can result in an [O II]/H$\alpha$ ratio below 2.5, which translates to [O II]/H$\beta$ < 7. Our measurements of [O II]/H$\beta$ alone thus cannot rule out ionization from an evolved stellar population.

We further investigated the locations of our emission-line ETGs in the colour–magnitude diagram and compared them with those of the other EDisCS ETGs. Following the same approach used
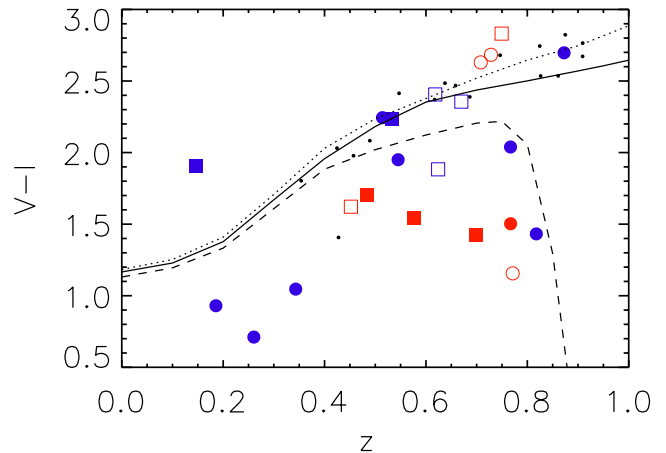


**Figure 2.** We compare the $V - I$ observer frame colour and redshift data for both the cluster (red) and field (blue) ETGs with the evolutionary synthesis models of Bruzual & Charlot (2003, lines). As in Fig. 1, ellipticals are represented as circles, S0s as squares, kinematically disturbed galaxies as open symbols, and undisturbed ones as filled symbols. Note that no magnitude or redshift cuts were applied to the plotted sample. The black dashed line corresponds to a 'formation redshift' (resdhift of last star formation episode) of $z_F \sim 0.9$, the solid line to $z_F \sim 1.5$, and the dotted line to $z_F \sim 2.5$, as in Jaffé et al. (2011a, fig. 12). All models assume solar metallicity ($Z_{solar} = 0.02$). For reference, the smaller black points correspond to the ETGs with 'artificial emission' (i.e. galaxies whose apparent emission is an observational artefact, see Section 3.1).

in Jaffé et al. (2011a), we used colours that were the nearest to rest-frame $U - V$ ($R - I$ for most clusters, and $V - I$ for the lowest redhift clusters), and found that some of the cluster ETGs displaying emission (kinematically disturbed and undisturbed) have colours that are consistent with the red sequence, but most are somewhat bluer.

For the field galaxies, we used the evolutionary synthesis models of Bruzual & Charlot (2003) to predict the observed $V - I$ colours of galaxies at different redshifts, assuming a passively evolving stellar population that formed in a single burst of 0.1 Gyr duration, as in Jaffé et al. (2011a). This is shown in Fig. 2 for different models, together with the observed $V - I$ colours of the field (blue symbols) and cluster (red) emission-line ETGs, that are also plotted for comparison. The different lines correspond to models computed with different times since the last star formation episode, $t_F$. Such look-back times can also be expressed in terms of a 'formation redshift', $z_F$ (see Jaffé et al. 2011a for details).

In Fig. 2, the emission-line ETGs have colours that are, on average, 0.3 mag bluer than the passive model lines. More precisely, almost half of these ETGs (47 per cent) have colours bluer than this average, and the colours can be up to 1 mag bluer than the models. Such colours can be explained by a small amount of ongoing or recent star formation, involving as little as ~5 per cent of the galaxy stellar mass, happening in the past ~1 Gyr. The exact amount of recent star formation required, naturally depends on the detailed star formation history of the galaxies and the time of observation. Our estimate however is reasonable for a broad range of star formation histories (see e.g. Barger et al. 1996).

In addition to colours, we looked at the Balmer absorption (H$\delta$ and H$\gamma$) strength and the 4000 Å break ($D_{n, 4000}$) of the galaxies, as they are sensitive to the galaxies' star formation histories. They are also less susceptible to reddening than rest-frame optical colours. Measures of these quantities are described in Rudnick et al. (in preparation), but we note here that the line strengths were

measured by decomposing the emission and absorption following Moustakas et al. (2010). In their paper, Rudnick et al. examine the [O II] emission of galaxies with old stellar populations, as defined by their EW(H$\delta$+H$\gamma$)/2 and $D_n$(4000). They distinguish 'young', 'intermediate', and 'old' stellar populations based on the luminosity-weighted stellar age sequence seen in the EW(H$\delta$+H$\gamma$)/2–$D_n$(4000) plane (see e.g. Kauffmann et al. 2003), and through the comparison with stellar evolution synthesis models. They conclude from their study that the ionized gas observed likely stems from a combination of mass-loss and accretion, and is stripped by ram-pressure in clusters.

When placing our emission-line ETGs in the $D_n$(4000) versus EW(H$\delta$+H$\gamma$)/2 diagram of Rudnick et al., we find that most (69 per cent) of the emission-line ETGs are consistent with having young-to-intermediate stellar populations, whilst only 4 (out of 13) galaxies are consistent with having 'old' stellar populations. Note that, given that most of our galaxies have evidence of significant recent star formation, they would not all have been included in Rudnick et al.'s sample. Nevertheless, more than half (13 out of 24) of our ETGs could be used in the comparison, and the characteristics of this sub-sample trace well the entire population of emission-line ETGs.

In sum, we conclude that star formation is the most likely explanation for the emission observed in most of the ETGs considered, although we cannot completely rule out the contribution of post-AGB stars or AGN to the ionization of all (or some) of the galaxies.

## 4.2 Environment

Across the full redshift and $M_B$ range of EDisCS galaxies, the emission-line ETG sample is dominated by field galaxies (62 per cent of the final sample, blue symbols in Fig. 1). Only nine emission ETGs were classified as cluster or group members (38 per cent, red symbols). This is partly because there are no EDisCS clusters at either $z \lesssim 0.35$ or at the highest redshifts, which leads to field galaxies outnumbering cluster galaxies in the EDisCS spectroscopic sample. However, the difference is small: 55 per cent of EDisCS galaxies are in the field, while 45 per cent are in clusters or groups. Moreover, if we take the matched sample region of Jaffé et al. (2011b, orange box in Fig. 1), which was defined to compare cluster and field galaxies, we find that emission-line ETGs are still predominantly field galaxies (70 per cent).

The field population is dominated by kinematically undisturbed galaxies, with only a third of field ETGs having distorted gas kinematics. In contrast, many of the cluster ETGs are kinematically disturbed galaxies, and also are all located towards the cluster outskirts, as shown in Fig. 3. The plot displays the projected distance to the cluster centre, $r/R_{200}$, on the $x$-axis, and the absolute value of the peculiar velocity, $|\Delta v/\sigma_{cl}|$, on the $y$-axis, where $\Delta v = v_{gal} - v_{cl}$, $v_{gal}$ is the line-of-sight velocity of the galaxy, $v_{cl}$ the central velocity of the cluster, and $\sigma_{cl}$ the cluster velocity dispersion. The grey points are all the cluster galaxies in EDisCS (defined as being within $\pm 3\sigma_{cl}$ from $z_{cl}$; Milvang-Jensen et al. 2008), the blue ones are the cluster spiral galaxies within the emission-line sample of (Jaffé et al. 2011b), and the red large symbols correspond to the cluster E/S0s discussed in this paper. As shown by the work of Mahajan, Mamon & Raychaudhury (2011) and Oman, Hudson & Behroozi (2013), and references therein, the location of galaxies in projected phase-space can give an idea of the time that the galaxies have spent in the cluster: within the bottom-left corner region in the plot, galaxies are mainly virialized, whilst the intermediate and outer regions (at higher velocities and/or distance to the cluster centre) contain a
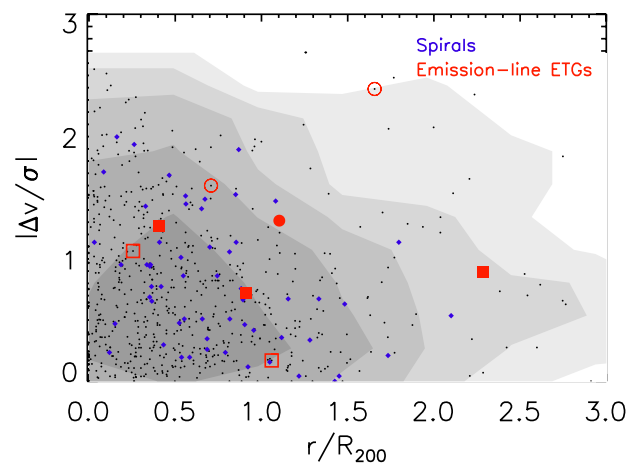


**Figure 3.** Stacked phase-space diagram ($r/R_{200}$ versus $|\Delta v/\sigma|$) for all the EDisCS cluster galaxies (black dots, no magnitude or redshift cuts were applied). The grey contours trace the number density distribution of the cluster galaxies, that concentrate, as expected, at low $r/R_{200}$ and $|\Delta v/\sigma|$. The emission-line galaxy sample with visual morphologies discussed in this paper is highlighted with larger coloured points. The smaller blue diamonds are the spiral population of emission-line galaxies. As in Fig. 1, the red circles and squares are elliptical and S0 galaxies, respectively. For the E/S0s, filled symbols trace galaxies with regular (rotating) emission and open circles disturbed kinematics. Interestingly, none of the cluster E/S0s in our sample are located in the virialized part of the cluster (bottom-left corner of the plot). Instead, they reside in the cluster infall region. Note that the galaxy EDCSN J1054525−1244189 is not plotted, as it belongs to a very low mass group (182 km s$^{-1}$ of velocity dispersion) with only 10 members, and hence, its phase-space position is not physically meaningful.

higher fraction of backsplash and infalling galaxies. The location of the few cluster ETGs with emission in phase-space indicates that they probably fell very recently into the cluster environment.

Our findings clearly indicate that ETGs with emission are preferably in the field, or in the outskirts of galaxy clusters.

## 4.3 Morphological disturbances

The ETGs considered in this paper are all elliptical and S0 galaxies with no strong signs of interaction or morphological distortions in their *HST* images. However, to identify the presence of small morphological disturbances undetected in our visual examination of the *HST* images, we visually inspected the residuals of single-Sérsic profile fits to the images, using the method described in Hoyos et al. (2011). This method is ideal to find interaction relics, as it enhances the residuals by subtracting the bulk of the smooth symmetric light. After this procedure, we identified eight ETGs with disturbed morphologies (20 per cent of emission-line ETGs, see column 9 of Table A1), five of which inhabit the field. Half of them have disturbed kinematics and the other half have regular disc kinematics; this is consistent with Jaffé et al. (2011b), where we found, using the entire emission-line galaxy sample, that disturbances in the gas distribution and kinematics are unrelated to morphological (stellar) disturbances. We emphasize that the disturbances discussed here are subtle and they do not represent major merger events or interactions.

The upper panels of Figs B1 and B2 show the morphologies and single-Sérsic fits for the final ETG sample separated by their kinematic properties (see Section 3.1).
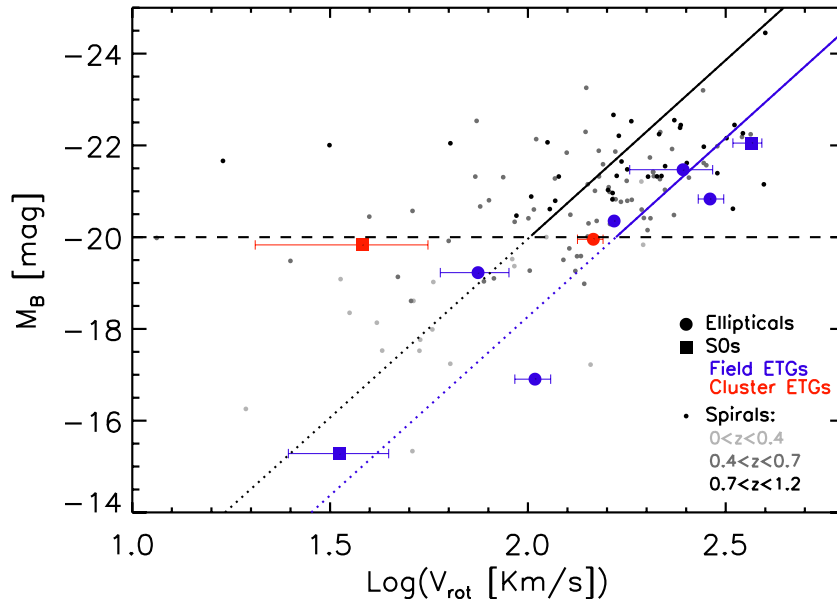
**Figure 4.** We compare the absolute-magnitude $M_B$ and rotation velocity data of EDisCS spirals (small symbols) and ETGs (bigger symbols). The spiral data are colour-coded in terms of redshift, as indicated in the bottom-right corner of the plot. Ellipticals (large solid circles) and lenticulars (large filled squares) are also distinguished. A red colour indicates that a galaxy is in a cluster/group environment, while blue corresponds to the field. We do not make redshift or magnitude cuts to the plotted sample, although we do not plot galaxies with velocities and velocity uncertainties consistent with no rotation (See galaxies labelled with † in Table A1). The solid lines correspond to the fitted TFR assuming the slope of Tully et al. (1998) and considering either the median shift in $M_B$ for the spiral galaxies brighter than $M_B = -20$ (black solid line), or the ETGs brighter than the same value (blue solid line). This value represents the magnitude limit above which below which the completeness is constant across the redshift range considered. For reference, we also show the relations extrapolated to the fainter galaxy magnitudes (dotted lines).

## 4.4 The Tully–Fisher relation

We present the TFR of emission-line ETGs and compare them to the spiral relation. We use the kinematically undisturbed galaxies, as in Jaffé et al. (2011b), where we found that global environment does not affect the TFR. To check that these galaxies had non-zero rotation, we further rejected galaxies with $V_{rot} < 2\sigma_{V_{rot}}^-$, where $\sigma_{V_{rot}}^-$ is the 95 per cent level uncertainty in the rotational velocity, $V_{rot}$ (see Jaffé et al. 2011b). 5 of our 14 kinematically undisturbed ETGs were consistent with no rotation and thus excluded from the TFR. The proportion of rejected galaxies does not depend on morphology, so applying this condition does not bias our results.

To construct the emission-line TFR, we derived galaxy inclinations by fitting a bulge and a disc to *F814W HST* images.[1] These two-component fits assumed that the bulge has a de Vaucouleurs profile and the disc an exponential profile, both convolved to the PSF of the images. This was done using the GIM2D software (see Simard et al. 2002, 2009 for a detailed description of the method used). Inclinations were used to correct absolute magnitudes for internal extinction (see Tully et al. 1998) and compute rotation velocities.

We emphasize that presence of a 'disc' component does not necessarily imply that there is an actual stellar disc, because many dynamically hot systems have simple exponential profiles. We also note that there might be slight biases in the inclination corrections $(\sin(i))$ applied to the emission-line rotational velocities because the galaxy inclinations were measured for the galaxy stellar-light distributions. This could cause an overestimation of the rotation velocity

of ellipticals that, unfortunately, cannot be accounted for. Moreover, the gaseous disc may not have a similar stellar counterpart.

Fig. 4 shows the *B*-band TFR of the spiral galaxies in the parent sample (small dots), as well as that of ETGs (larger symbols). Although we plot all the galaxies without any redshift or magnitude cut, to make a fair comparison between the spiral and ETG samples we only consider galaxies with $M_B < -20$ and we colour-code the spiral galaxies by redshift (see Fig. 1 for justification).

Despite the large scatter, it is clear that, for the $M_B$-limited sample, the emission-line ETGs are fainter than their spiral counterparts at a fixed rotational velocity. Applying the same slope found by Tully et al. (1998) for local galaxies, we fit the TFR by computing the median shift in $M_B$ (for galaxies with $M_B \leq -20$), for the EDisCS spiral (solid black line) and ETG (solid blue line) populations separately. The dotted lines are only extensions of the bright TFR to fainter magnitudes for reference. The difference between the spiral and ETG *B*-band TFRs is 1.7 mag in the bright regime.

The rest-frame *B* band is sensitive to both stellar population age and recent/current star formation, which could indicate that, if the emission in ETGs is caused by star formation (see discussion in Section 4.1), this is significantly lower than that found in spirals.

It has been shown that the scatter about galaxy scaling relations can be reduced by analysing the ratio between the rotational velocity and the galaxy velocity dispersion ($V_{rot}/\sigma$, e.g. Kassin et al. 2007; Zaritsky 2012). Utilizing this quantity, Zaritsky (2012) illustrated how all S0s (as well as ellipticals as $V_{rot}/\sigma$ increases) deviate away from the Fundamental Plane. This is also true for the TFR, where they find that S0s can be shifted to the spiral relation when adding the pressure term. As mentioned in Section 3.1, we cannot retrieve information about the velocity dispersion from our spectra. We note, however, that the dependence on the pressure term is only important when studying stellar kinematics. In this paper, we do

---

[1] The two-component fit performed to derive inclinations is independent of the single-Sérsic fit made to the *HST* images to examine possible interaction relics (Section 4.3).

not consider stellar dynamics but instead use emission lines (gas) to study rotation.

### 4.5 Specific star formation rates

If we assume that star formation is the main cause of the emission in the ETGs considered in this paper (see discussion in Section 4.1), we can investigate their star formation properties by using [O II]3727 Å emission as a star formation proxy. We cannot use other estimators such as Hα, which is not in our spectral coverage, or infrared (IR) data, because the available far-IR images only detect very high levels of star formation ($\gtrsim 10.3\,M_\odot\,yr^{-1}$ at $z = 0.6$; Vulcani et al. 2010) and none of the ETGs of this paper were detected.

We use the SFRs, uncorrected for dust, presented in Poggianti et al. (2008) when available. These fluxes were obtained by multiplying the observed [O II] equivalent width by the continuum flux, estimated from the broad-band photometry using total galaxy magnitudes. We further compute sSFRs by normalizing the SFR by stellar mass (as in Vulcani et al. 2010). We note that the sSFRs computed here are upper limits, as some (if not most) of the ionization could come from post-AGB stars or AGN, as discussed in Section 4.1.

Fig. 5 shows the sSFR as a function of stellar mass for the spirals and ETGs considered in this paper. Most of the ETGs have moderate-to-low sSFR in comparison with spirals. At the mean stellar mass (= $5.63 \times 10^{10}\,M_\odot$), the sSFR of high-redshift spirals is ∼4 times higher than that of ETGs. And if we take the intermediate-redshift galaxies, the difference is still a factor of 2. Most strikingly, our cluster emission-line ETGs are typically much less massive on average than field emission-line ETGs, and the field emission-line ETGs have the lowest sSFRs. The low sSFRs found in the ETGs, together with their red colours, are consistent with their location in the TFR.

Our results are in line with Verdugo, Ziegler & Gerken (2008), who found that cluster ellipticals at $z = 0.25$ have lower sSFRs than cluster spirals. Intriguingly, they also detect emission lines in the spectra of some of their red sequence cluster galaxies, for which they, however, lacked morphological information. They find that the sSFRs of these emission-line red sequence galaxies are between
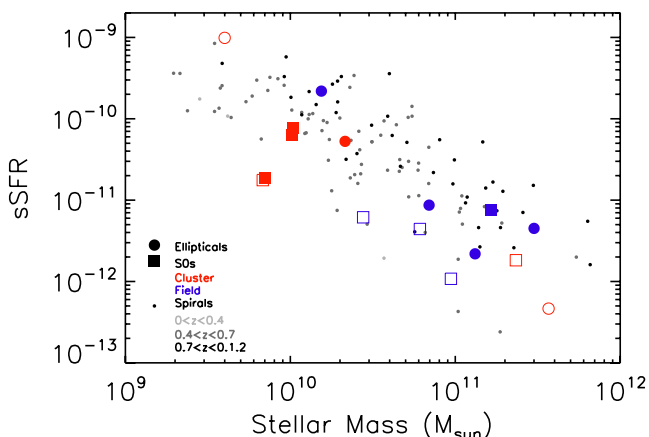


**Figure 5.** Stellar mass versus sSFR (uncorrected for dust) for the same spiral galaxies (small dots) and ETGs (bigger symbols). As in Fig. 4, the spirals are colour-coded according to their redshift, and the ETGs are blue if in the field, red if in a cluster/group, filled if undisturbed kinematics, open if disturbed, circle if elliptical and square if S0. No redshift or magnitude cuts were applied to the plotted sample.

those of ellipticals and spirals. We can speculate that their objects might be lower redshift analogues of our emission-line ETGs.

Moreover, our results agree with the SAURON study of ETGs in the local Universe (Shapiro et al. 2010), who found that nearly all star-forming ETGs fall below the main sSFR–stellar mass sequence of actively star-forming galaxies, but nonetheless have more star formation activity than the quiescent population.

## 5 DISCUSSION

Despite the difficulties imposed by the high-redshift nature of our sample, we have found clear evidence for the existence of ETGs with extended (sometimes rotating) ionized gas. Our findings are in agreement with low-redshift studies of elliptical and S0 galaxies (e.g. Trager et al. 2000; Cappellari et al. 2011), making this sample the first higher redshift analogue of the population of ETGs with complex ISM seen in the local Universe.

Two main questions arise from the finding of ETGs with ionized gas: Where did the gas come from, and what ionizes it?

Considering the latter question, the spectral properties of the galaxies under study suggest that star formation is the most likely explanation for the ionization observed. However, we cannot completely rule out possible contributions from post-AGB stars or AGN activity (see Section 4.1).

As for the origin of the gas in ETGs, there are two possibilities: (a) acquisition from an external source, and (b) internal production via mass return into the ISM from evolved stars. These two hypothesis have been debated in the literature for years (e.g. Faber & Gallagher 1976; Sarzi et al. 2006). We discuss our results in the context of each scenario in the following.

(a) In the first scenario, field elliptical and S0s with extended emission acquired their gas after they acquired their morphology, from an external source. This is possible because they do not inhabit the hostile cluster environment that could have prevented gas accretion. Instead, in the field, galaxy–galaxy mergers are more likely to occur.

If we assume star formation to be the main source of ionization of the gas in these ETGs, the small amount of star formation that we find could thus be interpreted as a 'frosting' on top of the old stellar population that dominates these galaxies. This frosting could be caused by minor gas-rich mergers, as the morphologies of these ETGs do not appear to be perturbed. This scenario is in line with cold dark matter models of structure growth predicting minor mergers and gas accretion still at lower redshifts.

(b) However, the 'observed star formation' can also be explained by gas returned from previously formed stars, which is expected from stellar evolution models. We estimate that ∼20–40 per cent of the total stellar mass is returned as gas by the evolved stellar populations.[2] If this gas is retained by the galaxy, it can form a significant amount of stars, and drive substantial sSFR. For instance, a galaxy with a stellar mass of $10^{11}\,M_\odot$ will have ∼$0.3 \times 10^{11}\,M_\odot$ of gas returned. If all this gas were then converted into stars and the star formation episode lasts for 5 Gyr, the SFR would be $6\,M_\odot\,yr^{-1}$ (equivalent to sSFR =$6 \times 10^{-11}\,yr^{-1}$), which is higher than the values found for $10^{11}\,M_\odot$ galaxies (see Fig. 5). If we assume a more realistic case in which only a few per cent of the gas is efficiently transformed into stars, we obtain the sSFRs observed in our sample. In other words, gas recycling alone can explain the levels of star

---

[2] The exact value depends on the initial mass function assumed.

formation found in the ETGs considered. This is expected to be possible only in the field, because cluster environment can remove gas from galaxies by means of for example ram-pressure stripping. This scenario is consistent with (1) field galaxies retaining more gas, thus being more likely to form stars and (2) undisturbed field ETGs (solid blue symbols in Fig. 5) having higher sSFR than disturbed ETGs (open blue symbols), which have presumably experienced gas loss. If the gas has been accreted from an external source, the star formation of the kinematically disturbed galaxies would be expected to have been enhanced. However, some models predict a suppression of star formation, so we cannot completely rule out an external origin.

Our conclusions are also in agreement with the study of Rudnick et al. (in preparation), who concludes from a mass-selected sample of EDisCS old galaxies, that the ionized gas observed in these systems is potentially stripped by ram-pressure in clusters.

Future observations with current and future state-of-the-art facilities will unveil the origin of the gas in ETGs at increasingly high redshift. In particular, resolved 2D kinematics for both the stellar and gaseous components in these high-redshift objects can place strong constraints in these galaxies' history.

## 6 SUMMARY AND CONCLUSIONS

We have studied the properties of the gas and the stars in a sample of 24 emission-line E/S0 galaxies from the EDisCS in different environments at $0 < z < 1$. Our main findings are as follows.

(i) ETGs with extended emission represent a significant fraction ($\geq 12$ per cent) of the emission-line galaxy population at $z < 1$.

(ii) We explore the possible ionizing sources of the gas in the ETGs at $z < 1$, such as AGN activity, star formation, and post-AGB stars, and favour star formation as the most likely cause of the observed emission.

(iii) Many of the emission-line ETGs have colours consistent with the old stellar populations found in the red sequence. However, 47 per cent have colours that are bluer than 0.3 (and up to 1) mag from the model predictions for passive evolution after a burst of star formation. This implies that there is a small amount of on-going or recent ($\lesssim 1$ Gyr) star formation, involving as little as $\sim 5$ per cent of the galaxy's stellar mass.

(iv) These emission-line ETGs are only found in the field and infall regions of clusters. This has different implications, depending on the origin of the gas:

(a) If the gas was acquired via interactions with other galaxies, this gas will be longer-lived outside the harsh cluster environment. This result is in agreement with the idea that ram-pressure strips the gas in galaxies at the centres of clusters.

(b) If instead the gas has an external origin, it is reasonable to expect to detect it in galaxies inhabiting the field or cluster outskirts, as they are the most likely places to host galaxy–galaxy interactions.

(v) Some (20 per cent) of the ETGs with emission show signs of moderate interaction in their stellar light, but most are unperturbed ellipticals or S0s. This indicates that, if the gas has an external origin, it was acquired after the galaxy had already achieved its current morphology and in a process gentle enough not significantly affect that morphology.

(vi) We analyse the TFR of the emission-line ETGs and compare them with EDisCS spirals, taking a matched range of redshifts, $M_B < -20$, and excluding galaxies with large velocity uncertainties. We find that EDisCS emission-line ETGs are $\sim 1.7$ mag fainter (in the rest-frame $B$ band) than spirals at a fixed rotational velocity. This result is consistent with local TFR studies, suggesting that ETGs have lower mass-to-light ratios than spirals since their light is dominated by older stellar populations.

(vii) Assuming star formation to be the main source of ionizing radiation, we find that, at fixed stellar mass, cluster emission-line ETGs have lower sSFRs than spirals, and field emission-line ETGs have, in general, the lowest sSFRs of the entire emission-line galaxy population in EDisCS. We emphasize, however, that our emission-line ETGs have higher SFRs than typical ETGs. Our results agree with low-redshift studies such as that of Verdugo et al. (2008) and Shapiro et al. (2010).

The analysis presented here constitutes an important step forward towards the understanding of the evolution of the complex ISM in ETGs by significantly extending the look-back-time baseline of such studies which have until now concentrated almost exclusively on low-redshift samples. Observations with current and future state-of-the-art facilities will reveal further details about the ISM in ETGs at increasingly higher redshifts.

## REFERENCES

Annibali F., Bressan A., Rampazzo R., Zeilinger W. W., Vega O., Panuzzo P., 2010, A&A, 519, A40
Aragón-Salamanca A., Ellis R. S., Couch W. J., Carter D., 1993, MNRAS, 262, 764
Baldwin J. A., Phillips M. M., Terlevich R., 1981, PASP, 93, 5
Barger A. J., Aragon-Salamanca A., Ellis R. S., Couch W. J., Smail I., Sharples R. M., 1996, MNRAS, 279, 1
Baum W. A., 1959, PASP, 71, 106
Bedregal A. G., Aragón-Salamanca A., Merrifield M. R., 2006, MNRAS, 373, 1125
Binette L., Magris C. G., Stasińska G., Bruzual A. G., 1994, A&A, 292, 13
Boselli A. et al., 2005, ApJ, 629, L29
Bower R. G., Lucey J. R., Ellis R. S., 1992, MNRAS, 254, 601
Bruzual G., Charlot S., 2003, MNRAS, 344, 1000
Cappellari M. et al., 2011, MNRAS, 416, 1680
Demoulin-Ulrich M.-H., Butcher H. R., Boksenberg A., 1984, ApJ, 285, 527
Desai V. et al., 2007, ApJ, 660, 1151
di Serego Alighieri S. et al., 2013, A&A, 552, A8
Djorgovski S., Davis M., 1987, ApJ, 313, 59
Dressler A., Lynden-Bell D., Burstein D., Davies R. L., Faber S. M., Terlevich R., Wegner G., 1987, ApJ, 313, 42
Faber S. M., Gallagher J. S., 1976, ApJ, 204, 365
Faber S. M., Dressler A., Davies R. L., Burstein D., Lynden-Bell D., 1987, in Faber S. M., ed., Nearly Normal Galaxies. From the Planck Time to the Present. Springer-Verlag, New York, p. 175
Finkelman I., Brosch N., Funes J. G., Kniazev A. Y., Väisänen P., 2010, MNRAS, 407, 2475
Forman W., Schwarz J., Jones C., Liller W., Fabian A. C., 1979, ApJ, 234, L27
Fritz A., Böhm A., Ziegler B. L., 2009, MNRAS, 393, 1467

Gerhard O., Kronawitter A., Saglia R. P., Bender R., 2001, AJ, 121, 1936

Gonzalez A. H., Zaritsky D., Dalcanton J. J., Nelson A., 2001, ApJS, 137, 117

Gopal-Krishna, Mhaskey M., Wiita P. J., Sirothia S. K., Kantharia N. G., Ishwara-Chandra C. H., 2012, MNRAS, 423, 1053

Halliday C. et al., 2004, A&A, 427, 397

Hoyos C. et al., 2011, MNRAS, 411, 2439

Jaffé Y. L., Aragón-Salamanca A., De Lucia G., Jablonka P., Rudnick G., Saglia R., Zaritsky D., 2011a, MNRAS, 410, 280

Jaffé Y. L. et al., 2011b, MNRAS, 417, 1996

Jørgensen I., Chiboucas K., Flint K., Bergmann M., Barr J., Davies R., 2006, ApJ, 639, L9

Kassin S. A. et al., 2007, ApJ, 660, L35

Kauffmann G. et al., 2003, MNRAS, 341, 54

Kehrig C. et al., 2012, A&A, 540, A11

Kewley L. J., Geller M. J., Jansen R. A., 2004, AJ, 127, 2002

Kim D.-W., 1989, ApJ, 346, 653

Macchetto F., Pastoriza M., Caon N., Sparks W. B., Giavalisco M., Bender R., Capaccioli M., 1996, A&AS, 120, 463

Mahajan S., Mamon G. A., Raychaudhury S., 2011, MNRAS, 416, 2882

Maraston C., Thomas D., 2000, ApJ, 541, 126

Milvang-Jensen B. et al., 2008, A&A, 482, 419

Moustakas J., Kennicutt R. C., Jr, Tremonti C. A., Dale D. A., Smith J.-D. T., Calzetti D., 2010, ApJS, 190, 233

Oman K. A., Hudson M. J., Behroozi P. S., 2013, MNRAS, 431, 2307

O'Sullivan E., Forbes D. A., Ponman T. J., 2001, MNRAS, 328, 461

Phillips M. M., Jenkins C. R., Dopita M. A., Sadler E. M., Binette L., 1986, AJ, 91, 1062

Poggianti B. M. et al., 2006, ApJ, 642, 188

Poggianti B. M. et al., 2008, ApJ, 684, 888

Rawle T. D., Lucey J. R., Smith R. J., Head J. T. C. G., 2013, MNRAS, 433, 2667

Renzini A., 2006, ARA&A, 44, 141

Rowlands K. et al., 2012, MNRAS, 419, 2545

Rudnick G. et al., 2009, ApJ, 700, 1559

Saglia R. P. et al., 2010, A&A, 524, A6

Sánchez-Blázquez P. et al., 2009, A&A, 499, 47

Sarzi M. et al., 2006, MNRAS, 366, 1151

Sarzi M. et al., 2010, MNRAS, 402, 2187

Shapiro K. L. et al., 2010, MNRAS, 402, 2140

Simard L. et al., 2002, ApJS, 142, 1

Simard L. et al., 2009, A&A, 508, 1141

Stasińska G. et al., 2008, MNRAS, 391, L29

Thomas D., Maraston C., Bender R., Mendes de Oliveira C., 2005, ApJ, 621, 673

Trager S. C., Faber S. M., Worthey G., González J. J., 2000, AJ, 120, 165

Trinchieri G., di Serego Alighieri S., 1991, AJ, 101, 1647

Tully R. B., Fisher J. R., 1977, A&A, 54, 661

Tully R. B., Pierce M. J., Huang J., Saunders W., Verheijen M. A. W., Witchalls P. L., 1998, AJ, 115, 2264

van der Wel A., Franx M., van Dokkum P. G., Rix H.-W., 2004, ApJ, 601, L5

Verdes-Montenegro L., Yun M. S., Williams B. A., Huchtmeier W. K., Del Olmo A., Perea J., 2001, A&A, 377, 812

Verdugo M., Ziegler B. L., Gerken B., 2008, A&A, 486, 9

Visvanathan N., Sandage A., 1977, ApJ, 216, 214

Vulcani B., Poggianti B. M., Finn R. A., Rudnick G., Desai V., Bamford S., 2010, ApJ, 710, L1

White S. D. M. et al., 2005, A&A, 444, 365

Williams M. J., Bureau M., Cappellari M., 2010, MNRAS, 409, 1330

Yan R., Blanton M. R., 2012, ApJ, 747, 61

Yan R., Newman J. A., Faber S. M., Konidaris N., Koo D., Davis M., 2006, ApJ, 648, 281

Yi S. K., Lee J., Sheen Y.-K., Jeong H., Suh H., Oh K., 2011, ApJS, 195, 22

Zaritsky D., 2012, ISRN Astron. Astrophys., 2012, 189625

Zaritsky D., Gil de Paz A., Bouquin A. Y. K., 2014, ApJ, 780, L1

Ziegler B. L., Bower R. G., Smail I., Davies R. L., Lee D., 2001, MNRAS, 325, 1571

## APPENDIX A: DATA TABLE

Table A1 lists the main properties of all the ETGs described in Section 3.

## APPENDIX B: MORPHOLOGIES AND KINEMATICS

In the following, we show the postage-stamps of the *HST* images, single-Sérsic models, emission lines in the optical spectra and the respective 2D emission-line fit for the 24 galaxies with E/S0 morphology and real emission spectra. As in Table A1, we separate the sample into kinematically disturbed and undisturbed galaxies (Figs B2 and B1, respectively).

**Table A1.** The emission-line ETG sample considered in this paper is listed in the first 24 rows. At the bottom, the galaxies with artificial emission (i.e. galaxies whose apparent emission is an observational artefact, see Section 3.1), and the galaxies that were misclassified as ETGs are also listed for reference. The columns are: EDisCS name, environment ('c' for cluster, 'f' for field and 'g' for group), redshift, absolute *B*-band magnitude, rotational velocity, flag for emission-line kinematics ('good' is undisturbed, 'dist' is disturbed, and 'bad' is artificial emission), Morphology, flag for morphological disturbance ('good' is undisturbed, 'dist' is disturbed). When an entry has '–' it means there is no data available. In addition, for ETGs with real emission (first 24 rows), we include 3 extra columns indicating their effective radii ($r_{eff}$, computed from the single-Sérsic fits), the ration between the spatial extent of the emission ($r_{extent}$, see Jaffé et al. 2011b for details and $r_{eff}$, and the equivalent width of the [O II] doublet.

| Object ID (EDCSNJ*) | Envi-. ronment | $z$ | $M_B$ (mag) | $\log V_{rot}$ (km s$^{-1}$) | Kinem. dist. | Morph. | Morph. dist. | $r_{eff}$ (kpc) | $r_{extent}/r_{eff}$ | EW[O II] (Å) |
|---|---|---|---|---|---|---|---|---|---|---|
| **Disc kinematics** | | | | | | | | | | |
| 1103485−1247452 | f | 0.7668 | −20.50 | $1.19^{+0.54}_{-INDEF}$ | Good | E | Dist†† | – | – | 23.511 |
| 1138115−1135008 | f | 0.1857 | −16.90 | $2.02^{+0.04}_{-0.05}$ | Good | E | Good | 0.81 | 3.35 | – |
| 1138170−1131411 | f | 0.2605 | −19.23 | $1.87^{+0.08}_{-0.10}$ | Good | E | Dist | 1.05 | 3.81 | – |
| 1227507−1139384† | f | 0.8725 | −22.66 | $1.58^{+0.39}_{-INDEF}$ | Good | E | Good | 4.48 | 1.80 | 9.45 |
| 1227577−1137211 | f | 0.5451 | −20.83 | $2.46^{+0.03}_{-0.03}$ | Good | E | Good | 3.57 | 2.93 | 9.869 |
| 1228026−1139163† | f | 0.3431 | −17.46 | $1.05^{+0.30}_{-INDEF}$ | Good | E | Good | 0.63 | 10.69 | – |
| 1354055−1234136 | f | 0.5142 | −21.47 | $2.39^{+0.07}_{-0.13}$ | Good | E | Dist | 3.41 | 0.51 | 3.998 |
| 1354073−1233336 | c | 0.7670 | −19.95 | $2.17^{+0.02}_{-0.04}$ | Good | E | Good | 1.7 | 4.09 | 29.349 |
| 1354074−1233206 | f | 0.8177 | −20.35 | $2.22^{+0.01}_{-0.01}$ | Good | E | Good | 1.59 | 4.10 | 60.993 |
| 1037495−1246452† | f | 0.5327 | −22.05 | $2.57^{+0.03}_{-0.05}$ | Good | S0 | Dist | 6.18 | 0.95 | 17.178 |
| 1037553−1246380 | g | 0.5768 | −19.83 | $1.58^{+0.17}_{-0.27}$ | Good | S0 | Good | 1.64 | 2.92 | 30.476 |
| 1054207−1148130† | c | 0.6996 | −19.98 | $1.00^{+0.66}$ | Good | S0 | Good | 2.29 | 1.28 | 27.794 |
| 1138112−1135117† | c | 0.4842 | −18.36 | $0.88^{+0.53}_{-INDEF}$ | Good | S0 | Good | 1.62 | 1.26 | 19.429 |
| 1232274−1251372 | f | 0.1467 | −15.28 | $1.52^{+0.12}_{-0.13}$ | Good | S0 | Good | 1.26 | 2.27 | – |
| **Disturbed kinematics** | | | | | | | | | | |
| 1054525−1244189 | g | 0.7283 | −22.34 | – | Dist | E | Dist | 4.21 | 0.98 | 1.582 |
| 1354144−1228536_A | f | 0.8245 | – | – | – | E | – | – | – | – |
| 1354144−1228536_B | f | 0.8243 | – | – | – | E | – | – | – | – |
| 1354022−1234283 | c | 0.7711 | −20.29 | – | Dist | E | Good | 1.04 | 3.93 | 62.848 |
| 1040356−1156026 | c | 0.7081 | −21.69 | – | Dist | E | Good | 2.66 | 10.68 | 2.908 |
| 1040415−1156207 | f | 0.6240 | −19.32 | – | Dist | S0 | Good | 1.97 | 0.48 | 9.088 |
| 1054356−1245264 | c | 0.7493 | −21.89 | – | Dist | S0 | Dist | 2.49 | 1.50 | 5.807 |
| 1138069−1136160 | c | 0.4520 | −18.62 | – | Dist | S0 | Good | 2.08 | 1.278 | 15.312 |
| 1216446−1202358 | f | 0.6698 | −20.75 | – | Dist | S0 | Good | 1.47 | 3.33 | 8.773 |
| 1354107−1231236 | f | 0.6183 | −21.96 | – | Dist | S0 | Dist | 1.63 | 1.58 | 2.446 |
| **Artificial emission** | | | | | | | | | | |
| 1054339−1147352 | f | 0.8608 | −21.97 | – | Bad | E | Good | | | |
| 1103458−1243353 | f | 0.4275 | −20.12 | – | Bad | E | Good | | | |
| 1138116−1134448 | c | 0.4571 | −20.72 | – | Bad | E | Dist | | | |
| 1138204−1131417 | f | 0.9090 | −21.75 | – | Bad | E | Good | | | |
| 1216527−1202553 | f | 0.8263 | −21.45 | – | Bad | E | Good | | | |
| 1216541−1157559 | f | 0.8748 | −21.75 | – | Bad | E | Good | | | |
| 1216548−1158039 | f | 0.9827 | −21.46 | – | Bad | E | – | | | |
| 1227589−1135135 | c | 0.6375 | −22.91 | – | Bad | E | Good | | | |
| 1354139−1229474 | f | 0.6865 | −22.05 | – | Bad | E | Good | | | |
| 1354185−1234431 | f | 0.9092 | – | – | Bad | E | – | | | |
| 1037552−1246368 | c | 0.4245 | −20.93 | – | Bad | S0 | Dist | | | |
| 1040476−1158184 | f | 0.6171 | −20.85 | – | Bad | S0 | Good | | | |
| 1054436−1244202 | c | 0.7463 | −21.49 | – | Bad | S0 | Good | | | |
| 1103418−1244344 | f | 0.3539 | −19.94 | – | Bad | S0 | Dist | | | |
| 1103430−1245370 | f | 0.6584 | −21.64 | – | Bad | S0 | Dist | | | |
| 1227552−1137559 | f | 0.4893 | −21.22 | – | Bad | S0 | Dist | | | |
| 1232288−1250490 | c | 0.5470 | −22.30 | – | Bad | S0 | Good | | | |
| **Misclassified ETGs** | | | | | | | | | | |
| 1138086−1131416 | f | 0.5039 | −19.03 | $1.55^{+0.17}_{-0.27}$ | Good | Irr/Disc | Dist | | | |
| 1354049−1234087 | f | 0.6617 | −20.89 | $2.48^{+0.03}_{-0.03}$ | Good | Spiral | Good | | | |
| 1354176−1232261 | f | 0.4779 | −20.50 | $2.54^{+0.01}_{-0.01}$ | Good | Spiral | Dist | | | |

†These emission-line galaxies have velocities and velocity errors that makes them consistent with no rotation and are thus not plotted in the TFR of Fig. 4.
††This galaxy is at the edge of the *HST* image, and hence, we did not attempt a single-Sérsic fit to it.
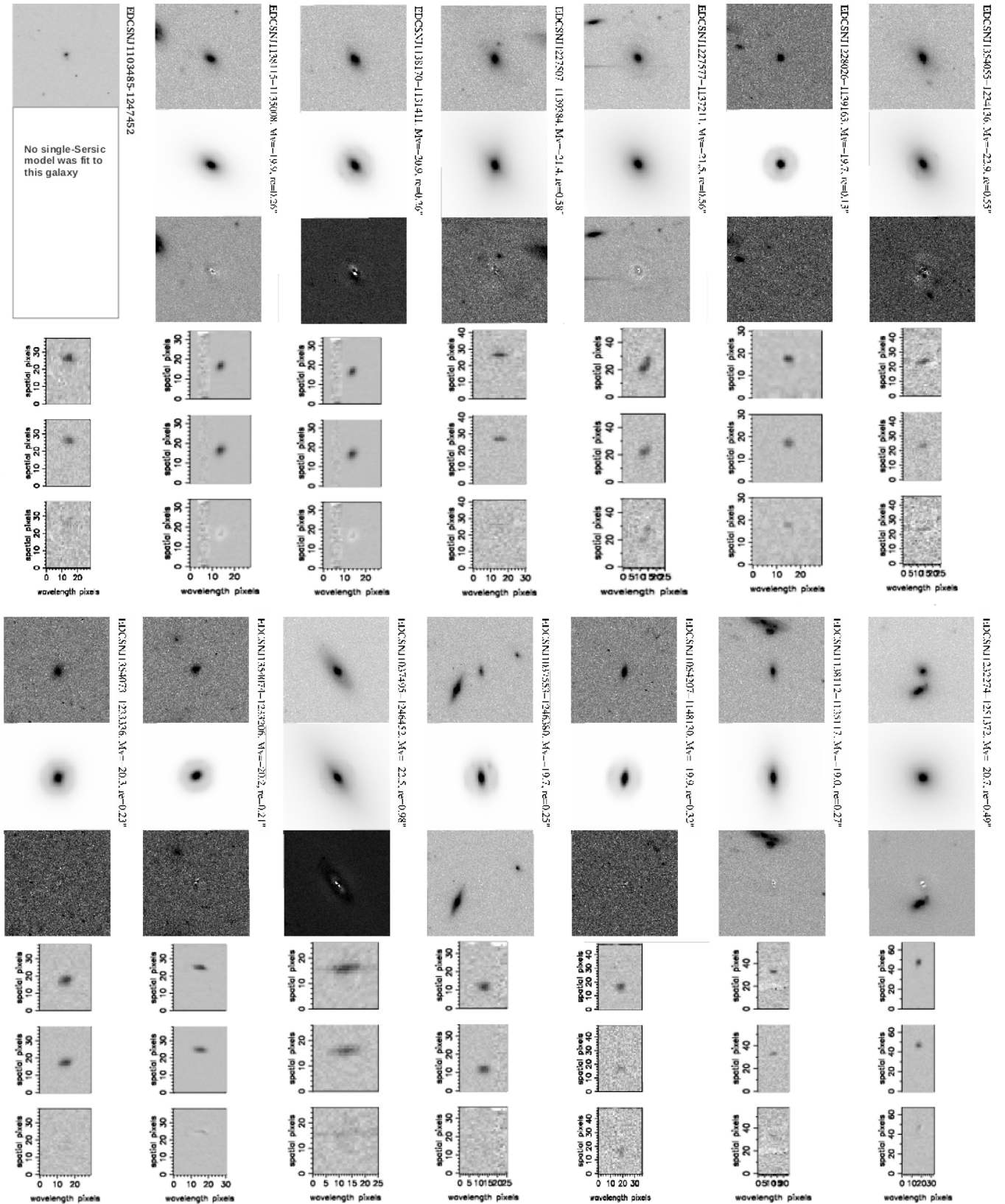
**Figure B1.** The 14 E/S0 in our sample showing signs of rotation in their gas emission (i.e. undisturbed kinematics) in two rows of six panels each. For each galaxy, the upper panel shows a 4 arcsec×4 arcsec *HST* image of the galaxy, the next panel the single-Sérsic fit, and the one below the residual image. The following three lower panels show the most prominent emission line, the 2D model, and the residual, respectively. The emission lines shown here are mostly the [O II]3727 Å doublet. When [O II]3727 Å was not available, the [O III]5007 Å line is shown instead (these cases can be identified by an '−' in column 11 of Table A1). Note that for the galaxy EDCSN J1103485−1247452 it was not possible to perform a good Single-Sérsic fit to it.
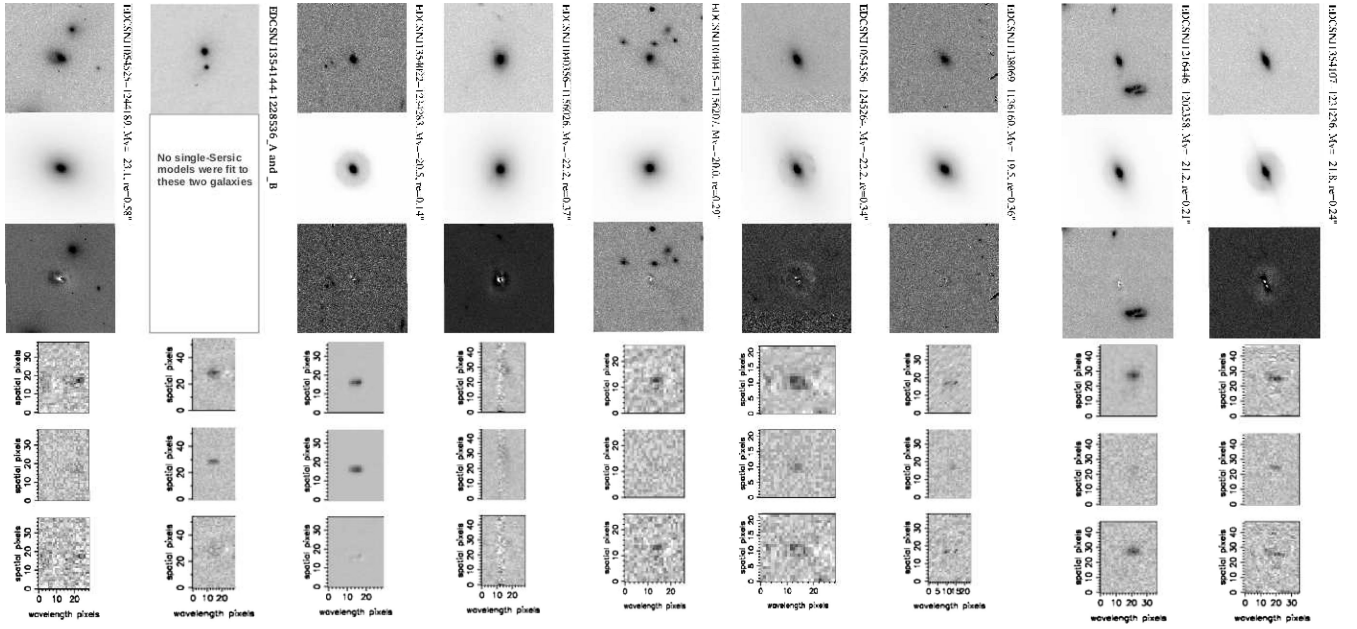
**Figure B2.** The 10 E/S0 in our sample showing extended emission but with disturbed gas kinematics. The panels are as in Fig. B1. Note that the pair EDCSN J1345144−1228536_A and _B are displayed together due to their vicinity.

This paper has been typeset from a TEX/LATEX file prepared by the author.